CATALYSIS

Overcoming limitations in propane dehydrogenation by codesigning catalyst-membrane systems

Rawan Almallahi[1,2], James Wortman[1,2], Suljo Linic[1,2]*

Propylene production through propane dehydrogenation (PDH) is endothermic, and high temperatures required to achieve acceptable propane conversions lead to low selectivity and severe carbon-induced deactivation of conventional catalysts. We developed a catalyst-membrane system that removes the hydrogen by-product and can thus achieve propane conversions that exceed equilibrium limits. In this codesigned system, a silica/alumina (SiO_2/Al_2O_3) hollow-fiber hydrogen membrane was packed with a selective platinum-tin (Pt_1Sn_1/SiO_2) PDH catalyst on the tube side with hydrogen diffusing from the tube to the shell side. We demonstrate that the catalyst-membrane system can achieve propane conversions >140% of the nominal equilibrium conversion with a propylene selectivity >98% without deactivation of the system components. We also show that by introducing oxygen on the shell side of the catalyst-membrane system, we can couple the endothermic PDH reaction on the tube side with exothermic hydrogen oxidation on the shell side. This coupling results in higher rates of hydrogen transport, leading to further enhancements in the propane conversion as well as desired thermoneutral system operation.

Propylene, used in the production of polypropylene, propylene oxide, and acrylonitrile (*1*), has been produced from petroleum through large-scale centralized steam and fluid catalytic cracking (*2*). However, the recent surge in shale gas has caused a shift in feedstock from naphtha to shale-based ethane. Steam cracking of ethane results in little to no propylene production, leading to the so-called propylene supply gap where the demand for propylene is projected to be higher than the supply (*3*).

One way to alleviate this problem is to develop technologies that can convert propane, another shale gas component, directly into propylene in a distributed fashion that is commensurate with the shale gas supply chain (*4*, *5*). A technology that meets these objectives is catalytic propane dehydrogenation (PDH), where propane is directly converted to propylene and hydrogen (H_2). PDH is an endothermic reaction requiring elevated reaction temperatures to achieve acceptable propane conversions (fig. S1). Under these high-temperature conditions, the rates of undesired side reactions, such as propane cracking and the formation of solid carbon on the catalyst surface, are more thermodynamically favored (fig. S2), leading to low selectivity and rapid catalyst deactivation, which requires frequent and costly catalyst regeneration (*6*–*9*). For example, the commercial Catofin chromium-based catalytic process alternates between dehydrogenation, regeneration, and purge steps within 15- to 30-min cycles (*10*). Various catalyst active site design strategies to increase activity and stability have recently been shown, and we refer to several review papers in this area for a more detailed summary (*1*, *2*, *11*).

Beyond the active site, coupling catalysis with separation functionality (for example, a permselective membrane) is a promising strategy for achieving outcomes that may not be attainable in traditional fixed- or fluidized-bed reactors (*12*–*14*). In the case of PDH, a strategy that specifically addresses the problem of low equilibrium conversion is to couple a PDH catalyst to a H_2-permeable membrane to form a catalyst-membrane chemical conversion system (*15*, *16*). In this design, H_2 molecules, formed during PDH, are removed from the reaction zone with a separation membrane that shifts the reaction equilibrium toward the product side and enhances propane conversion. This approach also reduces downstream separation requirements (separating propane and propylene is challenging) and costs. The membrane-catalyst system can also be operated at higher propane feed pressures, which is generally avoided because higher pressure leads to lower equilibrium conversions, so less catalyst and smaller reactor volumes can be used. Finally, lower operating temperatures may be possible, which would limit undesired high temperature cracking and catalyst-poisoning side reactions (*17*).

Despite these advantages, there are numerous obstacles to implementing this catalyst-membrane strategy. One obstacle is the limited availability of selective H_2-transporting membranes that can operate under these conditions. Previous studies have attempted to use metal-based (palladium) (*16*, *18*–*20*), zeolite (*20*–*22*), and oxide-based membranes (*16*, *18*, *23*, *24*) with very limited success owing to high cost, chemical reactivity that results in low product selectivity, and susceptibility to deactivation by carbon deposition (coking) under PDH conditions (*15*, *18*). In addition, commercial PDH catalysts are not viable for these systems because they are designed to operate with extra H_2 added to the reactant stream. For example, platinum (Pt)–based PDH catalysts (used in the Oleflex process) require additional H_2 to alleviate some of the problems with catalyst stability (*25*, *26*). This addition of H_2 is unsuitable for catalyst-membrane systems, which require a catalyst that can operate in a H_2-depleted regime (*27*).

We recently reported the development of a selective PDH catalyst that operates at the thermodynamic conversion limit with a propylene selectivity of >99% without any addition of H_2 (*28*). The catalyst consisted of small (~2 nm diameter) Pt_1Sn_1 nanoparticles (NPs) supported on silica (SiO_2) (*28*). In this work, we demonstrate the design of a multifunctional catalyst-membrane system that can operate at conversions that exceed the nominal thermodynamic limits of PDH at a given temperature. The catalyst-membrane system consists of the Pt_1Sn_1/SiO_2 PDH catalyst codesigned with a catalyst-compatible SiO_2-based H_2-permeable hollow-fiber membrane. We show that the membrane selectively removes H_2 produced during the PDH reaction on the catalyst, at meaningful removal rates, and shifts the PDH equilibrium toward a higher propane conversion and propylene yields.

We also discuss how the development of these catalyst-membrane systems allows us to expand the operational PDH temperature range to lower temperatures and incorporate exothermic oxidation of removed H_2 while retaining high conversion and reaction rates. This lower-temperature operation improved the stability of the materials from under the harsher, reducing catalyst-membrane system reaction conditions. Incorporating H_2 oxidation allows us to couple the endothermic PDH reaction on the tube side with the exothermic hydrogen oxidation on the shell side. This coupling results in higher rates of hydrogen transport, leading to further enhancements in the propane conversion as well as desired thermoneutral system operation. Finally, we shed light on several issues related to the development of efficient catalyst-membrane systems, demonstrating the need for the codesign and co-optimization of the catalytic and transport functionalities.

Catalyst-membrane design

An effective catalyst-membrane system relies on codesigning catalytic and separation functionalities to achieve optimal performance.

[1]Department of Chemical Engineering, University of Michigan, Ann Arbor, MI, USA. [2]Catalysis Science and Technology Institute, University of Michigan, Ann Arbor, MI, USA.
*Corresponding author. Email: linic@umich.edu

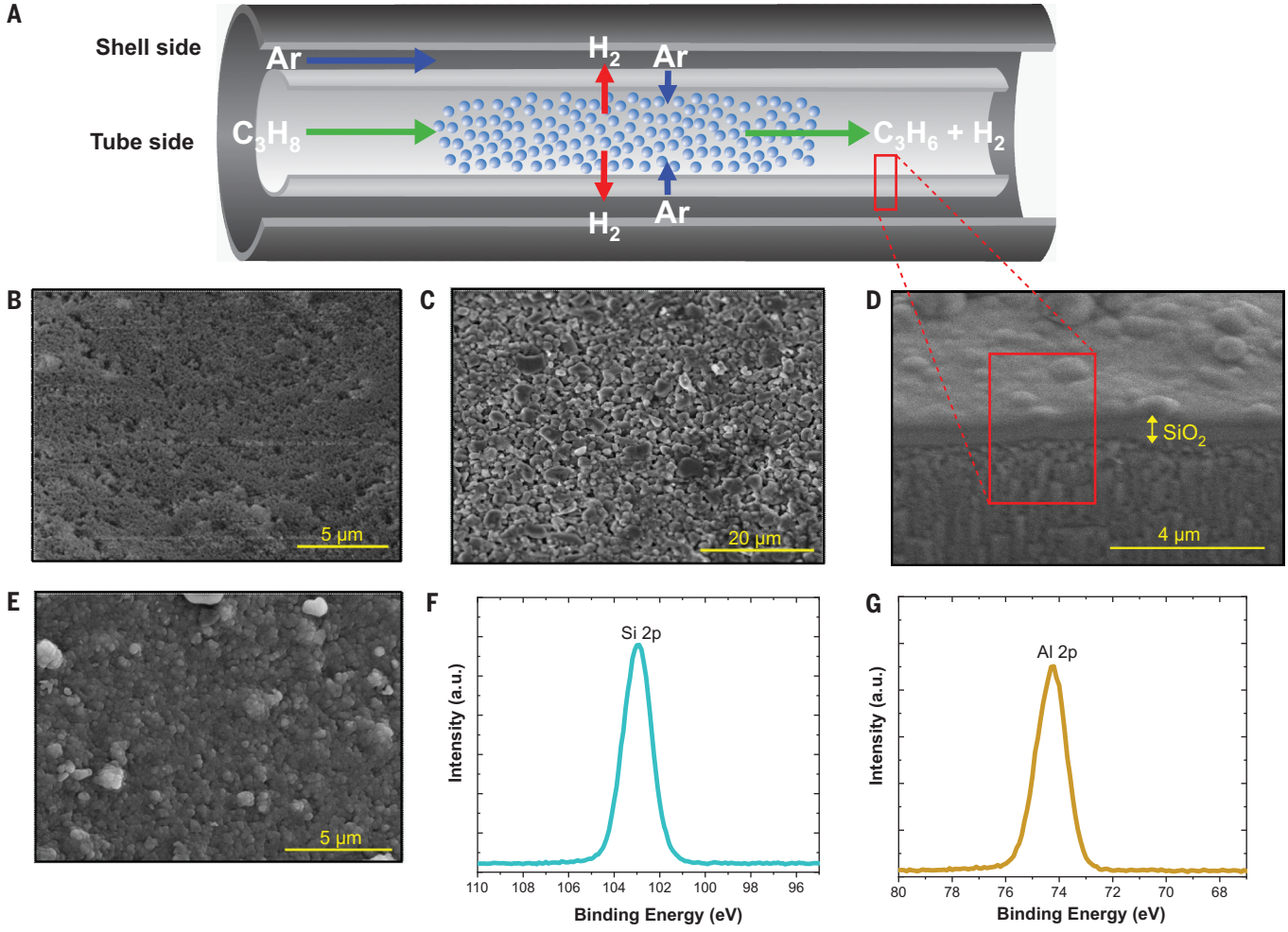

Fig. 1. Catalyst-membrane system and SiO_2/Al_2O_3 hollow-fiber membrane characterization. (**A**) Coupled catalyst-membrane system schematic. (**B**) Inner surface SEM image of the uncoated Al_2O_3 hollow-fiber membrane (before SiO_2 deposition). (**C**) Outer surface, (**D**) cross section, and (**E**) inner surface SEM images of the SiO_2/Al_2O_3 hollow-fiber membrane showing the porous Al_2O_3 substrate, layered SiO_2/Al_2O_3 structure, and the topmost smooth SiO_2 layer, respectively. (**F**) Si 2p photoemission spectra of SiO_2/Al_2O_3 hollow-fiber membrane. (**G**) Al 2p photoemission spectra of the uncoated Al_2O_3 hollow-fiber membrane.

A practical system should have high volumetric PDH reaction rates and high H_2-removal rates, so the membrane needs to have a high surface area for transporting H_2 without compromising catalyst surface area. This goal can be accomplished by using hollow-fiber membranes with small diameters packed with a PDH catalyst inside the hollow-fiber membrane. These hollow-fiber geometries allow for high membrane surface areas per volume of reactor (>1000 m^2/m^3), which can decrease overall reactor volumes to achieve desired conversions (*21*, *29*).

The catalyst-membrane hollow-fiber system (Fig. 1A) consists of an asymmetric and porous Al_2O_3 tubular hollow fiber with a thin SiO_2 separation layer on the inner side of the tube. The SiO_2 layer selectively separates H_2 from propane and propylene. The PDH catalyst was packed inside the fiber on the SiO_2 membrane side. The Al_2O_3 tube consisted of two Al_2O_3 layers (dimensions shown in fig. S3): an outer layer of ~860 μm with a 200-nm average pore size distribution, and an inner ~10-μm layer with a 20-nm average pore size distribution. The scanning electron microscopy (SEM) image of the inner surface in the Al_2O_3 tube shows a clear porous surface (Fig. 1B), whereas the SEM image of the outer surface shows large particles with a large pore size distribution (Fig. 1C). We deposited SiO_2 on the inner side of the Al_2O_3 tube through chemical vapor deposition (CVD) of tetraethyl orthosilicate (TEOS) at 600°C (figs. S4 to S6). A thin (~500 nm) SiO_2 separation layer formed on the inner side of the Al_2O_3 tube (Fig. 1D).

We established that the deposited SiO_2 covered the entire inner surface of the porous Al_2O_3 tube. The SEM image of the inner surface of the SiO_2/Al_2O_3 membrane (Fig. 1E) shows a smooth layer with a very small pore size distribution and no pinholes or cracks. The complete covering of the Al_2O_3 inner side with the SiO_2 separation layer was also confirmed using x-ray photoelectron spectroscopy (XPS). The XPS spectra associated with the characteristic Si 2p (Fig. 1F) and Al 2p peaks (Fig. 1G) for the SiO_2-coated and uncoated Al_2O_3 tubes, respectively, showed that no Al peaks were detected for the SiO_2-coated sample (see also figs. S7 and S8). The x-ray diffraction (XRD) pattern of the SiO_2/Al_2O_3 membrane in fig. S9 only showed the spectra for the Al_2O_3 substrate because the topmost SiO_2 layer was amorphous.

The PDH catalyst was composed of SiO_2-supported Pt_1Sn_1 NPs described previously (*28*). Approximately 250 mg of the Pt_1Sn_1/SiO_2 PDH catalyst was packed inside the hollow-fiber membrane on the tube side (where propane is fed), along the entire length of the tube. On the other side of the tube (shell side), an inert Ar sweep gas was used to carry the separated H_2.

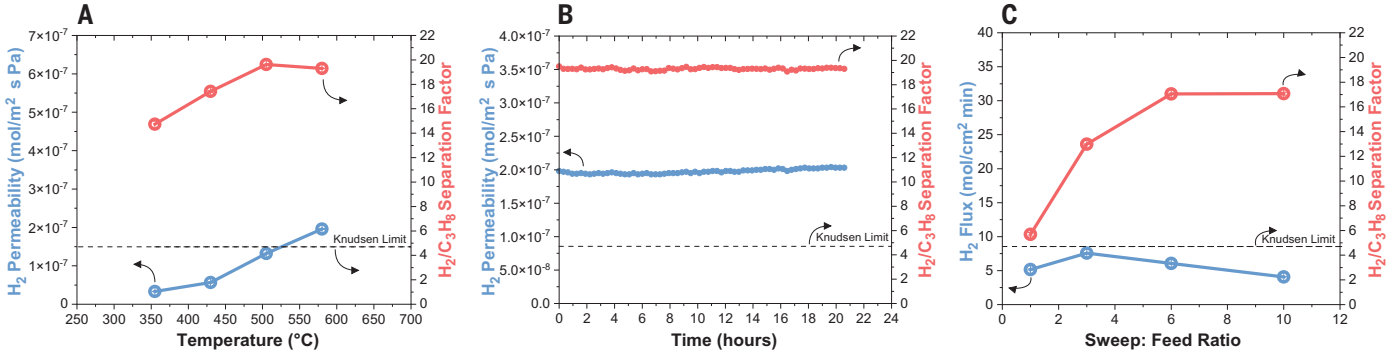

Fig. 2. SiO_2/Al_2O_3 hollow-fiber membrane characterization. (**A**) H_2 permeability and the H_2/C_3H_8 separation factor as a function of temperature; (**B**) time for an equimolar mixture of H_2 and C_3H_8 (5 cm^3/min each) and an Ar sweep on the shell side (60 cm^3/min); and (**C**) sweep:feed ratios (Ar sweep varied between 10 and 100 cm^3/min on the shell side) at T = 580°C. Error bars are the SD of multiple gas chromatography runs on the same membrane.

The SiO_2/Al_2O_3 membrane allows for some diffusion (backflow) of Ar to the inner tube side, so we needed to account for this backflow-induced dilution of the reactive mixture in the calculations of the equilibrium propane conversion.

Membrane performance

Data in Fig. 2 show the performance of the SiO_2-based membrane in separating H_2/C_3H_8 mixtures. Data in Fig. 2A show H_2 permeability and H_2/C_3H_8 separation factors measured at a total flow rate of 10 cm^3/min of an equimolar mixture of H_2/C_3H_8 at a sweep:feed ratio of 6. The sweep rate is the rate at which the inert sweep gas is moved on the shell side, removing gases that permeate through the membrane. At 580°C, where PDH is often operated, the SiO_2/Al_2O_3 hollow-fiber membrane exhibited a H_2 permeability of ~2×10^{-7} mol/m^2 s Pa and a H_2/C_3H_8 separation factor of 19.

The data in Fig. 2B show that the membrane performance was stable during the study (~20 hours). To put these separation factors in context, we compare them in Fig. 2C (and Fig. 2A) to the Knudsen separation limit, which represents the maximum separation that can be achieved by using the Knudsen effect. Our results show the SiO_2/Al_2O_3 hollow-fiber membranes exceeded these limits substantially. We attribute these high separation factors to two effects. First, the higher sweep-induced flow rate change created a driving force that drove H_2 through the membrane that was greater than the driving force to diffuse propane, so the partial pressure of H_2 (P_{H_2}) was lowered on the shell side. Second, molecular sieving occurred because the pores in the silica membrane were small enough to effectively exclude C_3 molecules and selectively diffuse only H_2. We refer to fig. S10 for details on deposition procedures for the membranes, and eqs. S1 to S3 for definitions of membrane performance metrics. For the hollow-fiber dimensions used herein, 60 min was chosen as the optimal deposition period for selective separation. Shorter deposition times were insufficient to fully coat silica on the fibers, whereas longer deposition times would introduce mass-transfer limitations.

Catalytic performance

Data in Fig. 3A show the performance of the catalyst-membrane system in PDH at 580°C, measured at pure propane feed (slightly diluted by Ar backflow discussed above), sweep:feed ratios between 4 and 10, and a constant weight hourly space velocity (WHSV) of 1.3 $hour^{-1}$. WHSV is defined as the mass of propane entering the reactor per unit time divided by the mass of the catalyst in the reactor. The different sweep:feed ratios were obtained by varying the Ar sweep gas flow rate on the shell side from 12 to 50 cm^3/min. We also show that the nominal thermodynamic limit on propane conversion under these reaction conditions (dashed black line) ranges between 50 and 52%, depending on the amount of Ar diluent present at the different sweep:feed ratios. The data show that at these conditions, the catalyst-membrane system reached propane conversions of ~10% higher (above 60%) than the equilibrium conversion with >95% propylene selectivity.

Another parameter that can be tuned to improve the H_2-removal rate is the WHSV, because at higher gas residence times (as the WHSV is lowered), a membrane can remove higher fractions of H_2 produced during the reaction. Data in Fig. 3B show the performance of the catalyst-membrane system for PDH at 580°C, pure propane feed (diluted by small amounts of Ar backflow), a constant sweep:feed ratio of 10, and with WHSVs changing from 0.86 to 2.16 $hour^{-1}$. The different WHSVs were obtained by varying the propane flow rate on the tube side between 2 and 5 cm^3/min for a constant catalyst loading of 250 mg. The data show that as WHSV decreased, propane conversion was substantially increased without sacrificing product selectivity.

Co-optimization studies

These multifunctional catalyst-membrane systems require co-optimization of multiple functionalities. In this case, the catalytic and the H_2 separation functions need to be codesigned, which requires concurrent tuning of multiple system parameters and creates a large design phase space that is difficult to explore. In these situations, it is useful to perform a dimensionless analysis to identify the minimal number of dimensionless variables that can guide the catalyst-membrane design. For catalyst-membrane systems, two dimensionless numbers, the Damkohler (Da) and Peclet (Pe) numbers, are sufficient to capture the design space (*30*–*33*). The Da number is described by the ratio of the reaction rate and the convective transport rate of the reactant through the reactor. It is closely related to the conversion that can be achieved in a system, with a larger Da number leading to larger conversion. The Pe number is the ratio of convective transport rate to the membrane permeation rate. A combination of high Da and low Pe numbers are desired for optimized performance, marked by a high reaction rate and a high H_2 permeation rate.

Data in Fig. 3C show the measured propylene yield in the catalyst-membrane system as a function of Da and Pe dimensionless numbers (calculated using eqs. S7 and S8). Those data were obtained at 580°C, with a pure propane stream (diluted by small amounts of Ar backflow). The Da and Pe numbers were varied by changing the WHSVs between 0.86 and 2.16 $hour^{-1}$ and sweep:feed ratios between 4 and 10. By changing the sweep:feed ratio, we changed the H_2 partial pressure difference across the membrane, which affected the Pe number, whereas changing WHSV affected both the Da and Pe numbers.

The data in Fig. 3C show that an improved performance is seen at higher Da and lower Pe (*29*, *30*) and that at 580°C, the highest propylene yield of 65% was achieved, which is

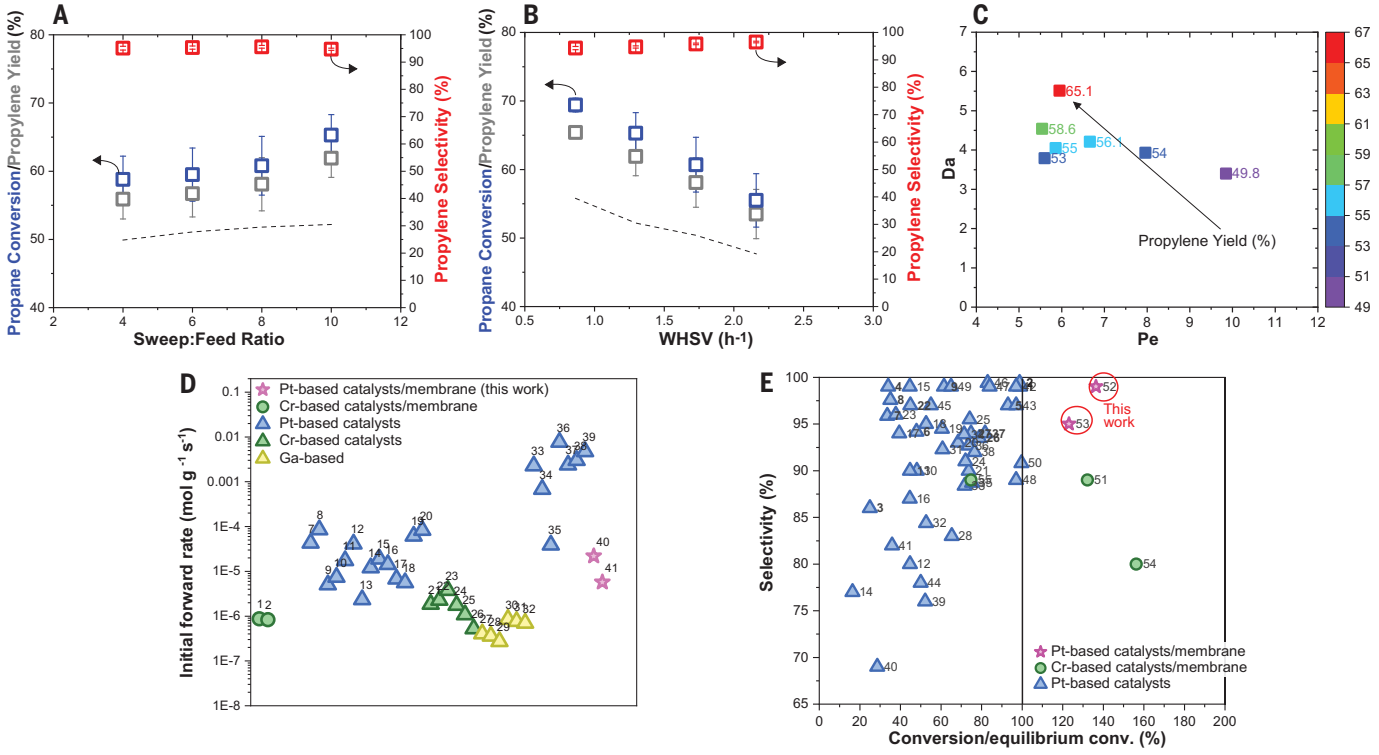

Fig. 3. Catalyst-membrane hollow-fiber system performance in propane dehydrogenation. (**A**) Propane conversion, propylene selectivity, and propylene yield as a function of sweep:feed ratios (WHSV = 1.3 hour^{-1}) compared to reaction equilibrium limit (dashed line) calculated for the same experimental conditions. (**B**) Propane conversion, propylene selectivity, and propylene yield as a function of WHSV (sweep:feed = 10) compared to reaction equilibrium limit (dashed line) calculated for the same experimental conditions. Error bars are the SD after replication of three catalyst loadings. (**C**) Propylene yield as a function of dimensionless Da and Pe. (**D**) Initial reaction rate for various membrane-catalyst systems and PBR catalysts reported in the literature. Numbers correspond to row numbers in table S1. Two data points from this work are for the catalyst-membrane system at 580° and 500°C (points 40 and 41, respectively). (**E**) Conversion–selectivity plots for different PDH catalysts. Numbers in the figure correspond to row numbers in table S2.

10% above the equilibrium limit (assuming 100% selectivity to propylene) of 55%. Therefore, we concluded that for the hollow-fiber catalyst-membrane tubular geometries analyzed herein, at 580°C, the enhancement factors in propylene yield, of ~10% above equilibrium conversion, are realistic. These enhancements could be further improved by making the diameter of the hollow-fiber membranes smaller or designing better-performing membranes; we note that there are reports of SiO_2-based membranes achieving two to three times higher H_2 permeability and separation factors of 500 or higher, which would further lower the Pe number (*34*).

To assess the practical utility of this multicomponent catalyst-membrane chemical conversion system, it is critical to compare it in a systematic way to its alternatives. A performance metric that is often used to quantify the performance of a catalyst is the forward rate of propane conversion per gram of the catalyst. We analyzed the inherent kinetic PDH reaction rates, using an integral reactor analysis (*28*), for many reported catalysts (*18*–*20*, *22*, *24*, *28*, *35*–*62*), and compared them to the rates measured on the Pt_1Sn_1/SiO_2 catalyst used in the membrane system herein. The data in Fig. 3D and table S1 show that the PDH rates in our system (pink stars) are comparable to the best-performing Pt-based PDH catalysts (blue triangles) and substantially higher than the rates on non-Pt–based materials (green and yellow symbols).

Another critical figure of merit in PDH is the selectivity to propylene as a function of propane conversion. Data in Fig. 3E and table S2 show the initial selectivity and conversion performance results for different reported PDH systems. The data show that the catalyst-membrane system analyzed herein outperformed other systems with respect to selectivity and conversion performance metrics. For example, at 580°C, the catalyst-membrane system reached ~123% propane conversion (relative to nominal equilibrium conversion) with >95% propylene selectivity. The performance could be even further improved relative to the thermodynamic equilibrium limit to >140% conversion with >98% propylene selectivity by lowering the temperature to 500°C. As shown in Fig. 3E, this performance exceeds other packed bed reactor (PBR) catalysts and catalyst-membrane systems previously tested for propane dehydrogenation, which in general suffer from poor selectivity or conversion (*20*, *22*–*24*).

Stability studies

Another crucial performance metric that has prevented serious commercial considerations for catalyst-membrane systems is their poor stability under carbon-rich, reducing PDH reaction conditions, which lead to formation of solid carbon deposits. These harsh conditions are further exacerbated by the removal of H_2. Previous studies of catalyst-membrane systems addressed these difficulties in several ways, such as substantially diluting the propane feed, reporting the initial time data points only, and often cofeeding H_2, which defeats the purpose of using the catalyst-membrane systems to shift equilibrium conversion (*17*–*20*, *23*, *24*).

Data in Fig. 4A show propane conversion, propylene selectivity, and yield as a function of time obtained with our Pt_1Sn_1/SiO_2 catalyst-membrane system at 580°C, in a pure propane stream, a WHSV of 1.3 hour^{-1}, and a sweep:feed ratio of 10. The catalyst-membrane system deactivated slowly over a time of ~22 hours. In table S1, we compared the rate of deactivation of the catalyst-membrane system discussed herein to the measured rates of deactivation of other systems [analyzed using first-order deactivation kinetics (*2*)]. The data in table S1 show that the

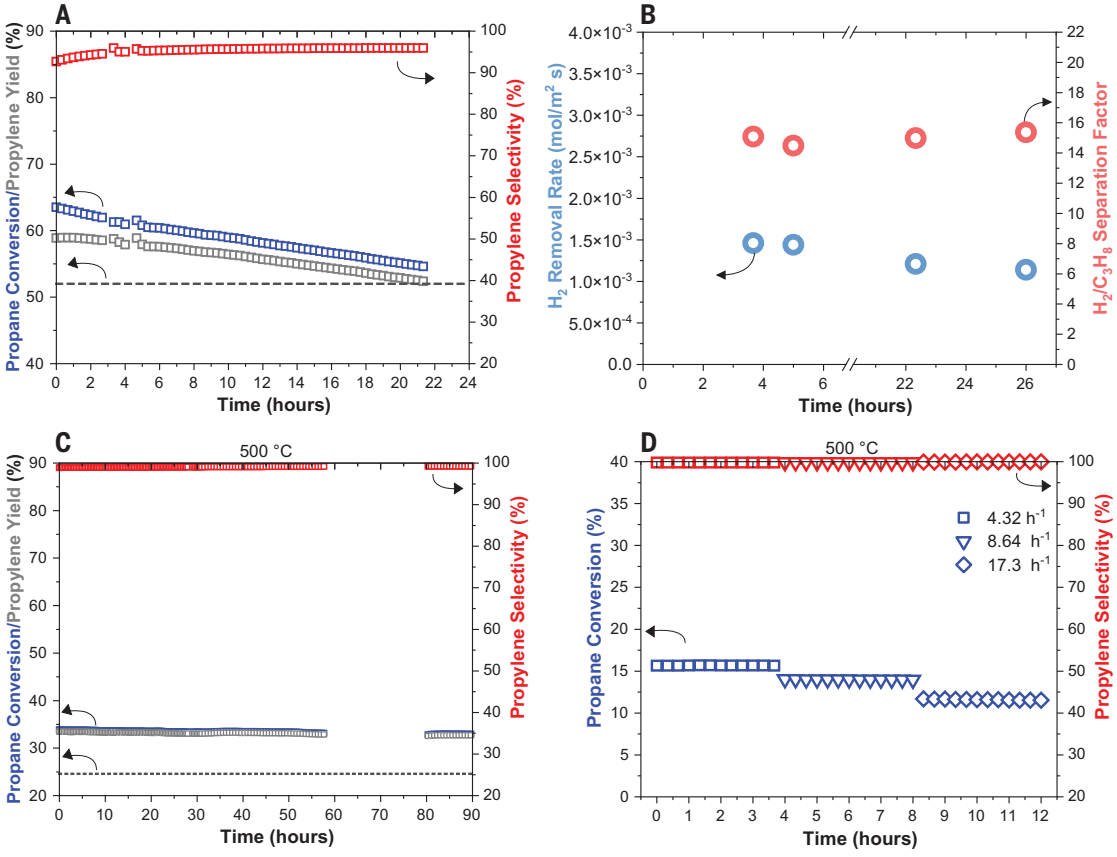

Fig. 4. Stability and low-temperature performance of catalyst-membrane hollow-fiber system. (**A**) Propane conversion, propylene selectivity, and propylene yield as a function of time for the catalyst-membrane hollow-fiber system compared to the equilibrium limit calculated for the same conditions (dashed line). (**B**) H_2-removal rate and the H_2/C_3H_8 separation factor as a function of time for the catalyst-membrane hollow-fiber system. For (A) and (B), reaction temperature = 580°C, $P_{C_3H_8}$ = 1 atm, WHSV = 1.3 hour^{-1}, and sweep:feed = 10. (**C**) Propane conversion, propylene selectivity, and yield as a function of time for the catalyst-membrane hollow-fiber system compared to the equilibrium limit calculated for the same conditions (dashed line). The missing data from ~58 to 80 hours were the result of a gas chromatography instrument gas tank running out over a weekend. Reaction temperature = 500°C, $P_{C_3H_8}$ = 1 atm, WHSV = 0.43 hour^{-1}, and sweep:feed ratio = 10. (**D**) Propane conversion and propylene selectivity as a function of time for the catalyst-membrane hollow-fiber system at different WHSVs. Reaction temperature = 500°C, $P_{C_3H_8}$ = 1 atm, and sweep flow rate = 100 cm^3/min.

stability of the Pt_1Sn_1/SiO_2 catalyst-membrane system, although not completely stable, exceeded the other catalyst-membrane systems, even those that resorted to feed dilution and cofeeding H_2 (*17*–*20*, *23*, *24*).

The decline in the performance of the catalyst-membrane system at 580°C (Fig. 4A) was likely related to a gradual deactivation of the catalyst as solid carbon formed on its surface, which is a general feature of PDH processes. This hypothesis was supported by data in Fig. 4B which show that the performance of the membrane was stable over time under the reaction conditions, that is, the measured H_2 removal rate and the H_2/C_3H_8 separation factor as a function of time were relatively constant. The slight decrease in the H_2-removal rate in Fig. 4B over time was the result of decreasing propane conversion that produced less H_2.

Carbon-induced deactivation in dehydrogenation catalysis can be limited by operating at lower temperature (*63*–*66*). An added benefit of lower-temperature operation is reduced energy input (*67*–*70*), but the main drawback is a decline in propane equilibrium conversion. We hypothesized that catalyst-membrane systems are ideal for lower-temperature operations, because higher propane conversions can be achieved at a specified temperature given that the catalyst-membrane systems can bypass equilibrium limits, as shown above and as simulated in fig. S11.

Data in Fig. 4C show propane conversion, propylene selectivity, and yield as a function of time at 500°C, in a pure propane stream, a WHSV of 0.43 hour^{-1}, and a sweep: feed ratio of 10 for the catalyst-membrane system (open blue and red squares). The data show that contrary to performance at 580°C, the system exhibited exceptional stability at these lower temperatures with >99% propylene selectivity. We compared the operation of the catalyst-membrane system to the thermodynamic equilibrium limit at 500°C. The data showed that the catalyst-membrane system operated above the equilibrium limit by ~9% higher conversion (~141% relative to equilibrium conversion) without noticeable deactivation for >90 hours on stream. This membrane-catalyst system achieved the same conversion at 500°C that would require 530°C, assuming the equilibrium conversion. The measured conversion levels at these conditions are comparable to those of commercial PDH processes, which are achieved at higher temperatures, and that suffer from rapid deactivation, even when operating with additional H_2 in the reactant stream (*1*).

More rigorous testing of catalyst stability requires that the system be antagonized under higher propane flow-rate conditions, i.e., at the conditions at which the catalyst is processing higher volumes of propane per unit time (away from equilibrium conversion). The data in Fig. 4D show that the catalyst-membrane system exhibited stable performance even as the flow rates increased. Expectedly, these increased flow rates led to lower conversions. In simple terms, our measurements show that at 500°C, the catalyst-membrane system is relatively stable with low deactivation rates at near 100% selectivity to propylene.

To further demonstrate the flexibility offered by this catalyst-membrane reactor systems designs, we explored coupling the propane dehydrogenation reaction on the tube side with the H_2 oxidation reaction on the shell side by introducing diluted O_2 in the sweeping gas (Fig. 5A). The introduction of O_2, which at these operating temperatures reacts with H_2 to form water, provides a twofold opportunity. One advantage is that it creates a larger driving force for the H_2 transport from the tube to the

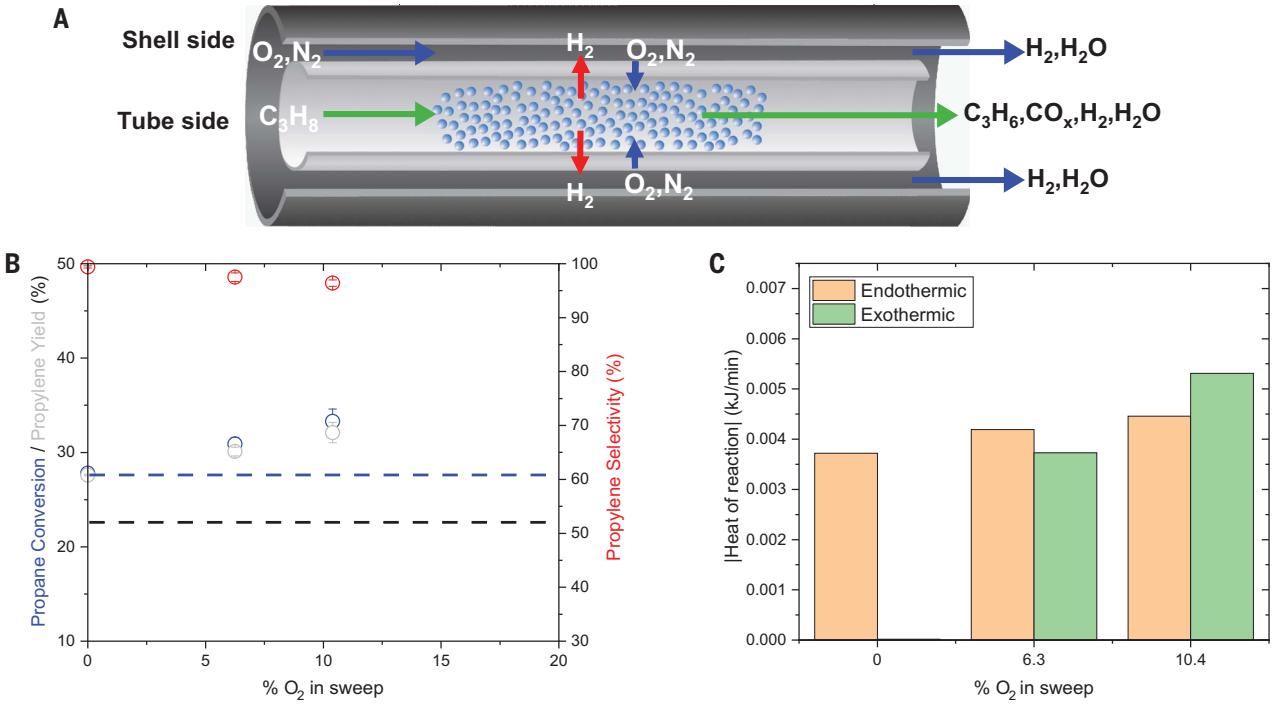

Fig. 5. Catalyst-membrane hollow-fiber system performance and heat calculations for propane dehydrogenation and coupled hydrogen combustion. (**A**) Coupled catalyst-membrane system for PDH and H_2 oxidation schematic. (**B**) Propane conversion, propylene selectivity, and propylene yield as a function of percent O_2 introduced in the inert sweep compared to the reaction equilibrium limit (dashed black line) and the case with no O_2 (dashed blue line). (**C**) Heat requirement for propane dehydrogenation and heat release from combustion of H_2 and propane oxidation as a function of percent O_2 introduced in the inert sweep. Reaction temperature = 500°C, $P_{C_3H_8}$ = 1 atm, WHSV = 0.86 hour^{-1}, and sweep:feed ratio = 12.

shell side because H_2 is consumed in the reaction with O_2. In addition, the exothermic H_2 oxidation provides heat for the endothermic PDH, i.e., the coupling of the two reactions could allow for a thermoneutral operation. Data in Fig. 5B show the performance of the catalyst-membrane system measured at 500°C for a pure propane feed on the tube side, sweep:feed ratio of 12 with 0 to 10% molar O_2 concentration in the sweep gas, and a constant WHSV of 0.86 hour^{-1}. The total sweep gas flow rate was maintained at 24 cm^3/min for experiments performed with different amounts of O_2.

The data show that in a pure N_2 sweep (no O_2 added), the catalyst-membrane system reached a propane conversion of ~28% (marked by the dashed blue line), which is 6% above the equilibrium conversion, with >99% propylene selectivity. After O_2 was introduced in the N_2 sweep on the shell side, higher propane conversions were obtained, reaching ~34% for 10% O_2. Under these conditions, propylene selectivity was very high: about 96.5% based on the carbon balance. We hypothesize that these greater propane conversions were the result of increasing H_2 removal from the tube to the shell side because of the consumption of H_2 by O_2 in the oxidation reaction (see fig. S15 for hydrogen-removal rates). To support this hypothesis, we measured the molar ratio of H_2O to CO_2 formed in the reacting systems and found that it was between 3.5 and 4.2, which means that O_2 is mainly reacting with H_2 (i.e., on the shell side) because oxidation of propane or propylene would lead to ratios of 1.33 or 1, respectively. These data are shown in fig. S15. The addition of steam during PDH may help alleviate coke formation, although this was not the intent of this study (*2*, *71*).

Using measured water-formation rates, material balances, and reaction rates, along with tabulated heats of reactions for all endothermic and exothermic reactions taking place in the catalyst-membrane system, we performed an energy balance analysis to establish the conditions required for the thermoneutral operation (calculation details are included in the supplementary materials). The data in Fig. 5C show the energy required to sustain PDH and energy released from H_2 oxidation reactions as a function of the amount of O_2 in the sweep. When no O_2 was present (0% O_2), PDH required considerable energy to be sustained at these temperatures (orange vertical bar). As O_2 was introduced, and PDH conversion increased, the energy required to support the reactions was also increased. The data in the figure show that for this specific system and under these conditions (i.e, the measured rates of reactions and selectivity) when the concentration of O_2 in the sweep reached 10%, the energy released by H_2 oxidation (green bars) became sufficient to drive the endothermic PDH reaction. An important advantage of the hollow-fiber design is that moving energy (heat) through these systems should be facile and controllable given the small dimensions of the tubes.

Discussion

In conclusion, we demonstrate an approach toward codesigning a catalytic and separation functionality for PDH that allows us to move beyond equilibrium conversion limits. We also show that the catalyst-membrane systems permit us to expand the temperature range for viable operation, allowing us to decrease system deactivation due to carbon coking and to incorporate exothermic H_2 oxidation. Rigorous technoeconomic costs and benefit analysis of a catalyst-membrane system will be crucial to understand its practical utility. Adding a membrane to a PDH catalyst will increase the reactor unit complexity. Nonetheless, potential technoeconomic benefits of the membrane-catalyst PDH systems include (i) the ability to operate at higher pressures (and therefore lower Pt catalyst loadings and smaller reactor

volumes) compared to commercial PDH processes, which are operated only at 1 to 3 atm owing to equilibrium limitations; (ii) the ability to seamlessly integrate exothermic hydrogen oxidation on the permeate side, which would increase the H_2 permeation driving force and reduce the need for interstage heating; (iii) the possibility of achieving similar heat transfer benefits if steam is used as the sweeping fluid; and (iv) the decreased downstream separations cost associated with the demanding propane-propylene and C_3/H_2 separations. These factors, along with the enhancement in stability and viable temperature operating range demonstrated here, offer substantial opportunities for improving yields and energy efficiencies in PDH processes.

REFERENCES AND NOTES

1. S. Chen *et al*., *Chem. Soc. Rev.* **50**, 3315–3354 (2021).
2. J. J. H. B. Sattler, J. Ruiz-Martinez, E. Santillan-Jimenez, B. M. Weckhuysen, *Chem. Rev.* **114**, 10613–10653 (2014).
3. E. National Academies of Sciences and Medicine, *The Changing Landscape of Hydrocarbon Feedstocks for Chemical Production: Implications for Catalysis: Proceedings of a Workshop* (The National Academies Press, Washington, DC, 2016); https://www.nap.edu/catalog/23555/the-changing-landscape-of-hydrocarbon-feedstocks-for-chemical-production-implications.
4. Office of Oil and Natural Gas, *Office of Fossil Energy*, *"Natural Gas Flaring and Venting: State and Federal Regulatory Overview* (Trends, and Impacts, 2019).
5. R. Mansoor, M. Tahir, *Energy Fuels* **35**, 3675–3714 (2021).
6. Z.-J. Zhao, C. C. Chiu, J. Gong, *Chem. Sci.* **6**, 4403–4425 (2015).
7. F. Jiang *et al*., *ACS Catal.* **5**, 438–447 (2014).
8. J. Wang *et al*., *ACS Catal.* **11**, 4401–4410 (2021).
9. A. Iglesias-Juez *et al*., *J. Catal.* **276**, 268–279 (2010).
10. M. M. Bhasin, J. H. McCain, B. V. Vora, T. Imai, P. R. Pujadó, *Appl. Catal. A Gen.* **221**, 397–419 (2001).
11. M.-L. Sun, Z.-P. Hu, H.-Y. Wang, Y.-J. Suo, Z.-Y. Yuan, *ACS Catal.* **13**, 4719–4741 (2023).
12. J. Wortman, V. O. Igenegbai, R. Almallahi, A. H. Motagamwala, S. Linic, *Nat. Mater.* **22**, 1523–1530 (2023).
13. V. O. Igenegbai, R. Almallahi, R. J. Meyer, S. Linic, *ACS Energy Lett.* **4**, 1465–1470 (2019).
14. V. O. Igenegbai, R. J. Meyer, S. Linic, *Appl. Catal. B* **230**, 29–35 (2018).
15. J. N. Armor, *J. Membr. Sci.* **147**, 217–233 (1998).
16. H. Weyten, J. Luyten, K. Keizer, L. Willems, R. Leysen, *Catal. Today* **56**, 3–11 (2000).
17. Z. D. Ziaka, R. G. Minet, T. T. Tsotsis, *J. Membr. Sci.* **77**, 221–232 (1993).
18. J. P. Collins *et al*., *Ind. Eng. Chem. Res.* **35**, 4398–4405 (1996).
19. E. Gbenedio, Z. Wu, I. Hatim, B. F. K. Kingsbury, K. Li, *Catal. Today* **156**, 93–99 (2010).
20. S. Pati, N. Dewangan, Z. Wang, A. Jangam, S. Kawi, *ACS Appl. Nano Mater.* **3**, 6675–6683 (2020).
21. Z. Wang *et al*., *AIChE J.* **66**, e16278 (2020).
22. S.-J. Kim *et al*., *Chem. Mater.* **28**, 4397–4402 (2016).
23. R. Schäfer, M. Noack, P. Kölsch, M. Stöhr, J. Caro, *Catal. Today* **82**, 15–23 (2003).
24. H. Weyten, K. Keizer, A. Kinoo, J. Luyten, R. Leysen, *AIChE J.* **43**, 1819–1827 (1997).
25. C. Li, G. Wang, *Chem. Soc. Rev.* **50**, 4359–4381 (2021).
26. Q. Li *et al*., *Top. Catal.* **54**, 888–896 (2011).
27. A. Sattler *et al*., *Energy Environ. Sci.* **15**, 2120–2129 (2022).
28. A. H. Motagamwala, R. Almallahi, J. Wortman, V. O. Igenegbai, S. Linic, *Science* **373**, 217–222 (2021).
29. S.-W. Choi *et al*., *AIChE J.* **63**, 4519–4531 (2017).
30. S. Battersby *et al*., *Catal. Today* **116**, 12–17 (2006).
31. Y. V. Gokhale, R. D. Noble, J. L. Falconer, *J. Membr. Sci.* **103**, 235–242 (1995).
32. W. S. Moon, S. B. Park, *J. Membr. Sci.* **170**, 43–51 (2000).
33. S.-W. Choi *et al*., *AIChE J.* **61**, 922–935 (2015).
34. R. M. De Vos, H. Verweij, *Science* **279**, 1710–1711 (1998).
35. Z. Wu, I. M. D. Hatim, B. F. K. Kingsbury, E. Gbenedio, K. Li, *AIChE J.* **55**, 2389–2398 (2009).
36. O. A. Bariås, A. Holmen, E. A. Blekkan, *J. Catal.* **158**, 1–12 (1996).
37. J. Salmones, J.-A. Wang, J. A. Galicia, G. Aguilar-Rios, *J. Mol. Catal. Chem.* **184**, 203–213 (2002).
38. Y. Zhou, S. M. Davis, Low-Pressure Dehydrogenation of Light Paraffins, US Patent 5,214,227 (1993).
39. N. Kaylor, R. J. Davis, *J. Catal.* **367**, 181–193 (2018).
40. Y. Zhang, Y. Zhou, L. Huang, M. Xue, S. Zhang, *Ind. Eng. Chem. Res.* **50**, 7896–7902 (2011).
41. P. L. De Cola, R. Gläser, J. Weitkamp, *Appl. Catal. A Gen.* **306**, 85–97 (2006).
42. Y. Duan, Y. Zhou, Y. Zhang, X. Sheng, M. Xue, *Catal. Lett.* **141**, 120–127 (2011).
43. G. Siddiqi, P. Sun, V. Galvita, A. T. Bell, *J. Catal.* **274**, 200–206 (2010).
44. P. Sun, G. Siddiqi, W. C. Vining, M. Chi, A. T. Bell, *J. Catal.* **282**, 165–174 (2011).
45. D. Shee, A. Sayari, *Appl. Catal. A Gen.* **389**, 155–164 (2010).
46. F. J. Pérez-Reina, E. Rodríguez-Castellón, A. Jiménez-López, *Langmuir* **15**, 8421–8428 (1999).
47. M. Alcántara-Rodríguez, E. Rodríguez-Castellón, A. Jiménez-López, *Langmuir* **15**, 1115–1120 (1999).
48. X. Zhang, Y. Yue, Z. Gao, *Catal. Lett.* **83**, 19–25 (2002).
49. K. L. Fujdala, T. D. Tilley, *J. Catal.* **218**, 123–134 (2003).
50. J. J. H. B. Sattler *et al*., *Chem. Commun.* **49**, 1518–1520 (2013).
51. M. Saito, S. Watanabe, I. Takahara, M. Inaba, K. Murata, *Catal. Lett.* **89**, 213–217 (2003).
52. B. Zheng, W. Hua, Y. Yue, Z. Gao, *J. Catal.* **232**, 143–151 (2005).
53. P. Michorczyk, J. Ogonowski, *Appl. Catal. A Gen.* **251**, 425–433 (2003).
54. B. Xu, B. Zheng, W. Hua, Y. Yue, Z. Gao, *J. Catal.* **239**, 470–477 (2006).
55. M. Chen *et al*., *J. Catal.* **256**, 293–300 (2008).
56. L. Shi *et al*., *Angew. Chem.* **127**, 14200–14204 (2015).
57. E. J. Jang, J. Lee, H. Y. Jeong, J. H. Kwak, *Appl. Catal. A Gen.* **572**, 1–8 (2019).
58. H. Xiong *et al*., *Angew. Chem. Int. Ed.* **56**, 8986–8991 (2017).
59. L. Liu *et al*., *Nat. Catal.* **3**, 628–638 (2020).
60. L. Deng *et al*., *ChemCatChem* **6**, 2680–2691 (2014).
61. L. Deng, T. Shishido, K. Teramura, T. Tanaka, *Catal. Today* **232**, 33–39 (2014).
62. L. Liu *et al*., *Nat. Mater.* **18**, 866–873 (2019).
63. M. Larsson, M. Hultén, E. A. Blekkan, B. Andersson, *J. Catal.* **164**, 44–53 (1996).
64. M. P. Lobera, C. Téllez, J. Herguido, M. Menéndez, *Appl. Catal. A Gen.* **349**, 156–164 (2008).
65. H. P. Rebo, E. A. Blekkan, L. Bednářová, A. Holmen, in *Studies in Surface Science and Catalysis*, B. Delmon, G. F. Froment, Eds. (Elsevier, 1999), **vol. 126**, pp. 333–340; https://www.sciencedirect.com/science/article/pii/S0167299199804832.
66. M. van Sint Annaland, J. A. M. Kuipers, W. P. M. van Swaaij, *Catal. Today* **66**, 427–436 (2001).
67. P. Wang *et al*., *Appl. Catal. B* **300**, 120731 (2022).
68. Z. Song *et al*., *Ind. Eng. Chem. Res.* **59**, 17250–17258 (2020).
69. R. T. Hannagan *et al*., *Science* **372**, 1444–1447 (2021).
70. Y. Qu *et al*., *Eng.* **9**, 12755–12765 (2021).
71. G. Festa, P. Contaldo, M. Martino, E. Meloni, V. Palma, *Ind. Eng. Chem. Res.* **62**, 16622–16637 (2023).

ACKNOWLEDGMENTS

Funding: This material is based upon work supported by the US DOE Office of Basic Energy Sciences, Division of Chemical Sciences (DE-SC0021008). The initial work on the project was support by RAPID under Award no. DE-EE0007888. R.A. acknowledges support from the National Science Foundation Graduate Research Fellowship under grant no. DGE 1256260. The authors acknowledge the Michigan Center for Materials Characterization for technical support. **Author contributions:** S.L. and R.A. conceived the project and designed the experiments. R.A. and J.W. designed and constructed the reactor used to obtain reaction data. R.A. performed propane dehydrogenation experiments and membrane characterization. All authors analyzed the reaction data and membrane characterization data. S.L., R.A., and J.W. wrote the paper. All authors edited the manuscript. **Competing interests:** A provisional patent application has been filed for this work (U.S. Provisional Application Patent No. 63/378,234). The authors declare no competing interests. **Data and materials availability:** All other data needed to evaluate the conclusions in the paper are present in the paper or the supplementary materials.

SUPPLEMENTARY MATERIALS

science.org/doi/10.1126/science.adh3712
Materials and Methods
Figs. S1 to S15
Tables S1 and S2

Submitted 27 February 2023; resubmitted 23 November 2023
Accepted 8 February 2024
10.1126/science.adh3712